Interaction of the Monsoon and Pacific Trade Wind System at Interannual Time Scales. Part I: The Equatorial Zone

T. P. BARNETT

Climate Research Group, Scripps Institution of Oceanography, University of California, San Diego, La Jolla, CA 92093

(Manuscript received 27 September 1982, in final form 4 January 1983)

ABSTRACT

The time history of the Monsoon System over the Indian Ocean has been developed from ship observations and merged with the Wyrtki-Meyers Pacific Trade Wind field. The interaction of these two massive wind systems has been studied by a rather new empirical orthogonal function (EOF) analysis capable of detecting propagating features in the wind systems. The current study (Part I) was confined to variations within ±10° of the equator.

Results show the two wind systems are strongly coupled at interannual time scales. The coupling is effected through cyclostationary pulsations and longitudinal shifts of the huge surface convergence over Indonesia. The interaction may also be thought of as the spatial expansion/contraction of the wind systems. These changes can be viewed as the transition of the Monsoon/Trade Winds between two preferred climate states. One sub-element of this apparent bimodality in the wind fields is the El Niño phenomenon.

The zonal component of the combined wind fields seems to instigate the large-scale interaction noted above. Perturbations in the *u*-component are composed of two interesting elements. One is a traveling disturbance which moves from the Indian Ocean eastward into the Pacific, and has many features of an equatorially trapped Kelvin wave. The second is a standing wave pattern which has maxima in the Indian and western Pacific with a node over Indonesia (the Walker cell). These perturbations preceed El Niño events and are phase-locked to the seasonal cycle. Their time variation can be viewed as a frequency-modulated process. A quasi-biennial oscillation appears in both wind fields as a standing wave pattern with in-phase maxima off the east coast of Africa and west coast of South America.

Subsequent papers will describe the interaction of the Monsoon/Trade Winds system in the band ±30° of the equator (Part II) and, in Part III, build a mechanistic, physical picture for the results obtained in Parts I and II.

1. Introduction

The Pacific Trade Wind Field system has been studied extensively since the development by Wyrtki and Meyers (1975a,b) of a data set describing its variations over the last 30 years. The space/time character of the Trade Winds has been described (Barnett, 1977; Goldenberg and O'Brien, 1981) as has its disposition during different phases of the Southern Oscillation (Pazan and Meyers, 1982). The relation between the Trade Winds and the local wind system off South America has been described (Hickey, 1975; Enfield, 1981) while the dynamical relation between the Trade Winds and associated sea level pressure field has been explored by Egger *et al.* (1981). Unfortunately, all of these studies stop at 120°E longitude, the western limit of the Wyrtki and Meyers data set, and so do not consider the interaction between the Trade Winds and the Indian Monsoon System.

Oceanographers have been understandably interested in the relation between the Trade Winds and the entire El Niño phenomenon, (e.g., Cane and Sarachik, 1981; McCreary, 1976; Philander, 1979). The observed winds have been used to force simple numerical ocean models that have reproduced key features of the El Niño (Busalachi and O'Brien, 1981). The elements of the Trade Winds responsible for these successful simulations have been revealed by empirical studies. Hickey (1975) and Wyrtki (1975) suggest the importance to El Niño of low-frequency fluctuations in the Southeast Trades. Much stronger statistical and theoretical results point to changes in the zonal wind stress in the far western equatorial Pacific as being a prerequisite for El Niños (McCreary, 1976; Barnett, 1977, 1981). The statistical studies identify the region of prime importance to lay within the influence of both the Trade Winds and the Monsoon System. Again the western limit of 120°E on the Trade Winds data was a constraint on these studies.

The above results suggest the importance of investigating the interaction between the Trade Winds and Monsoon. Indeed, visual inspection of anomalies in the two fields suggested the "propagation" of information from the Indian Ocean into the Pacific region. Hence the importance of studying both wind systems simultaneously. Further, a complete picture of the surface wind field accompanying the Southern

Oscillation cannot be obtained without consideration of the Monsoon System. Finally, the region where the Monsoon/Trade Winds interact corresponds to the massive surface convergence zone over Indonesia. This area is of prime importance to the atmospheric energy balance through the large release of latent heat that occurs there. These reasons, plus other compelling climate questions, led to the current study. A similar analysis does not appear to have been made previously.

The present work is the first in a three-part series. The first two parts use a rather new anaysis technique to explore the space/time scales and propagation of information within the Monsoon/Trade Winds systems. Part I explores the zonal band within 10° of the equator, i.e., in an equatorial wave-guide, while Part II describes variations in the zone between 30°N and 30°S. These two analyses will yield somewhat different results. The climatological implications of Parts I and II results are presented in Part III which is a more physical, mechanistic interpretation of the previous results. The net result will be to present a somewhat different view of air/sea interactions in the tropics than is currently in vogue.

Subsequent sections of this paper describe briefly the construction of a time history of the Monsoon windfield over the Indian Ocean to 30°S. The analysis technique to be used on the combined Trade Winds/Monsoon data is described next. Following sections explore the behavior of the zonal and meridional wind components, as well as the variations in the vector field.

2. Data

a. Preliminary treatment

Ship observations from the Indian Ocean form the basis for the Monsoon data set. Individual ship reports, plus the Dutch contribution to the Historical Sea Surface Temperature set, were extracted for the region bounded by 40°S and the Asian continent, Africa and 130°E. The time period extended from 1947–78, with radioed ship reports (courtesy U.S. Naval FNOC) providing the post-1972 data. The distribution of observations was surprisingly good in both space and time; better than in the Pacific (Fig. 1).

The raw data were organized by 1° square and month. Wind speed values exceeding 40 m s^{-1} were deleted and the remaining data screened against a 4 standard deviation filter. The subsequent analysis technique (Section 3) strongly discriminates against small-scale noise, hence the rather light filtering of the raw data.

The data were next averaged into 2 × 10° quadrangles and bimonthly periods. This gave an adequately dense data field for analysis. Voids in this data set were filled by simple objective mapping techniques. Similar operations were performed on the Trade Winds set of Wyrtki and Meyers (1975a,b). The result of these operations was a gridded (2° × 10°) set of bimonthly wind vectors covering the ocean between ±30° of the equator, stretching from Africa to South America and spanning the period 1947–78. An example of these data in the zone ±10° of the equator is shown in Fig. 2a and confirms the fact that the original data are quite noisy. Prior to the early 1950's the data in the Pacific were so sparse as to be of questionable value and the present analysis will thus concentrate on the period 1952–78.

b. Seasonal cycle and anomaly fields

The seasonal cycle was next estimated for each grid point. Typical mean fields for two bimonths show the well known properties of the Trade Winds/Monsoon (Fig. 2b; cf. Sadler and Harris, 1970). During July–August the Northern Hemisphere summer monsoon

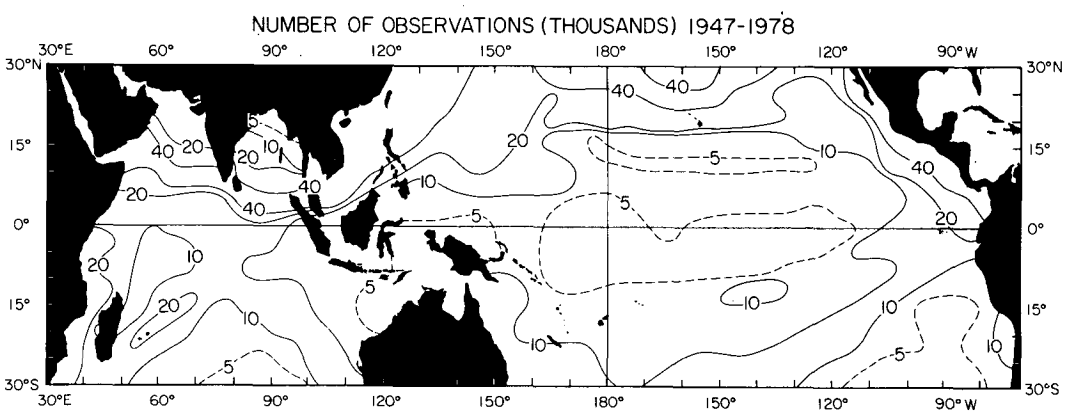

FIG. 1. Distribution of wind observations (in thousands).

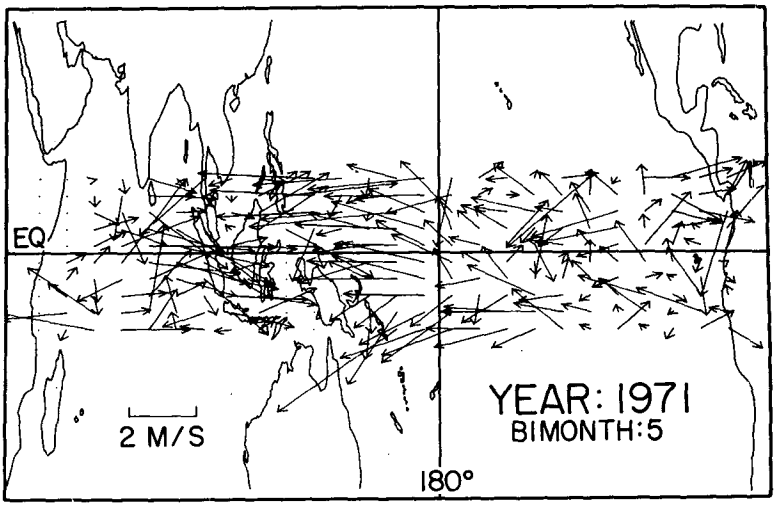

FIG. 2a. Example of raw anomalous vector wind data for bimonth 5 (September/October) of 1971.

is fully developed, reaching out of the Indian Ocean north of the equator and into the western equatorial Pacific. A marked convergence zone exists from north of Australia, over Indonesia and up along the coast of Southeast Asia. In the Southern Hemisphere, the flow is uniform and from the southeast over both the Pacific and Indian Oceans.

By contrast, late fall and Northern Hemisphere winter (January–February) see the intensification of the Northeast Trades and the penetration of northeasterlies over the entire Indian Ocean north of the equator. The strong convergence moves westward into the region of Sumatra and the eastern Indian Ocean. In the Southern Hemisphere the uniform southeasterly flow has retreated to 20°S. Strong convergence zones are established off the east coast of northern Australia and in the middle of the southern Indian Ocean.

The interannual variability at each grid point was obtained by subtracting the seasonal cycle at the grid point. Two interesting facts arose from this simple operation: 1) The seasonal cycle in the northern Indian Ocean appears to change its magnitude by order 30% on a decadal time scale. Independent wind data from islands in the area substantiated this fact. 2) The strength of the Trade Winds/Monsoon was higher between circa 1970–77 than at any other time during the study period. The former result causes some problems defining "anomalies" in the traditional sense. However, several different numerical treatments of the effect showed it had no appreciable impact on the current analysis and subsequent results of Sections 4–6. The subject will be treated in a separate study of the Monsoon System alone. The latter result, which has also been observed by O'Brien (personal communication), appears real and will be apparent in Sections 4–6.

3. Theory

a. General Approach

The problem is to investigate the interaction between the combined Monsoon/Trade Wind System. These dynamic systems move their regions of spatial influence seasonally. Further, their interaction may

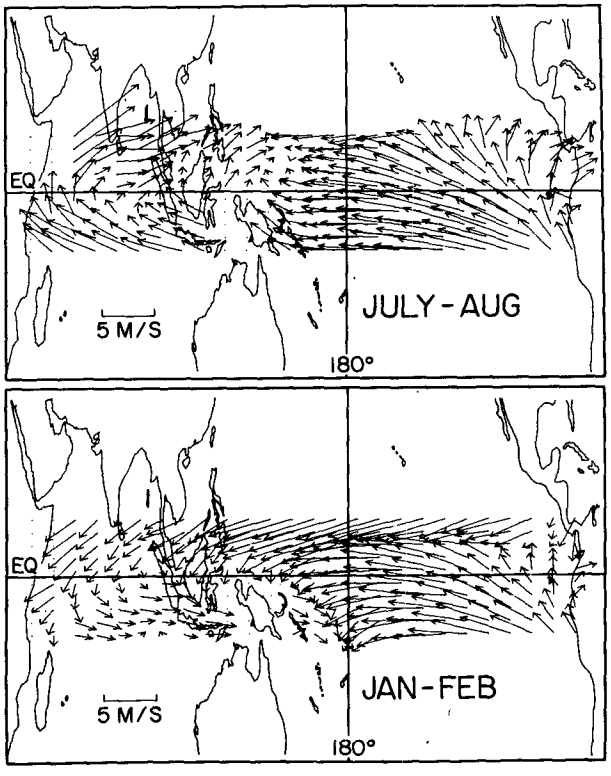

FIG. 2b. Long-term Monsoon/Trade Winds mean fields for January/February and July/August.

well involve propagation of information between them. Such a problem normally would be studied with cross-spectral analysis. Unfortunately, at least some elements of the interaction seem characterized by short-term, irregular "event" type features and/or cyclo-stationarity, such as phase locking of anomalies with the annual cycle (e.g., Hasselmann and Barnett, 1981; Meyers, 1982). Spectral analysis is inappropriate in such situations. The analysis method used was complex empirical orthogonal function (EOF) analysis and is carried out in the time domain. This method partially avoids the problems associated with conventional cross-spectral analysis in the nonstationary settings noted above.

The basic idea seems to have first appeared in Rasmusson *et al.* (1981), although its description there had some shortcomings. Earlier work by Wallace and Dickinson (1972) showed the potential of the complex analysis described below, although it was not really used by those authors. More recently Anderson (1982) used a variant of the approach on a study of atmospheric angular momentum distribution. The following discussion develops the theory of the method from fundamentals of Fourier theory and shows that the method provides much more information about a data field than has previously been discussed by the above authors.

We consider a scalar[1] field $u(x_j, t)$ where j is a spatial position index and t is time. Provided u is both simply and square integrable it has a Fourier representation of the form

$$u_j(t) = \sum_{\omega} a_j(\omega)\cos\omega t + b_j(\omega)\sin\omega t, \qquad (1)$$

where the Fourier coefficients (a, b) are defined in the usual manner.

Description of traveling features requires both co- and quadrature information. Such information is provided in the time domain by the complex representation of a variable, i.e.,

$$U_j(t) = \sum_{\omega} c_j(\omega)e^{-i\omega t}, \qquad (2)$$

where the Fourier-Stieltjes increment $c_j(\omega) = a_j(\omega) + ib_j(\omega)$ and $i = \sqrt{-1}$. Expanding (2) using this fact and collecting terms gives

$$U_j(t) = \sum_{\omega} \{[a_j(\omega)\cos\omega t + b_j(\omega)\sin\omega t] + i[b_j(\omega)\cos\omega t - a_j(\omega)\sin\omega t]\} = u_j(t) + i\hat{u}_j(t). \qquad (3)$$

The real part of (3) is just $u_j(t)$ from (1). The imaginary part of (3), $\hat{u}_j(t)$, is easily seen to represent $u_j(t)$ phase shifted $\pi/2$ in time and is called the quadrature function or Hilbert transform of $u_j(t)$ (e.g., Thomas, 1969). Formally

$$\hat{u}_j(t) = -\frac{1}{\pi}\int \frac{u(z)dz}{t-z}, \qquad (4)$$

where it is understood that the integration indicates the Cauchy principal value of the integral is taken. Comments on the Hilbert transform and means of estimating it in practice are given in the Appendix. For now we note: 1) $\hat{u}$ is roughly equivalent in the time domain to the quadrature spectrum in the frequency domain. This is so because the $\pi/2$ phase shift of each incremental Fourier component is equivalent to providing optimum lag information on that component. Thus, in a sense, U_j has built into it information on relative phase among the elemental sinusoids. 2) u and $\hat{u}$ are a natural transform pair whose interrelationships are well known (cf., Thomas, 1969) and they are orthogonal by construction.

b. *Signal detection and field descriptors*

The covariance matrix of $U_j(t)$ is given by

$$C_{jk} = \langle U_j^*(t)U_k(t)\rangle_t, \qquad (5)$$

where the asterisk denotes complex conjugation and $\langle\cdots\rangle_t$ indicates a time averaging process. Since C is the complex "zero lag" covariance matrix, it follows from standard spectral analysis theory that

$$C_{jk} = \int_0^{\omega_n} \phi_{jk}(\omega)d\omega, \qquad (6)$$

where ϕ_{jk} is the (complex) cross spectrum and ω_n the Nyquist frequency. Hence C_{jk} represents the cross-spectral matrix averaged over a specific frequency band and so will provide "blurred" information on traveling disturbances in that band. The frequency bandwidth of interest can be controlled easily by suitable filtering operations as noted in the Appendix.

The principal information in C is contained in its low-order eigenstructure. Now C is Hermitian by construction and so possesses real eigenvalues (λ_n) and complex eigenvectors, $B_n(\mathbf{x})$, where $\mathbf{x}$ represents spatial dependence. The corresponding EOF representation of U, which optimally accounts for variance in $u(\mathbf{x}, t)$ in the frequency band under study, is

$$U(\mathbf{x}, t) = \sum_n A_n(t)B_n^*(\mathbf{x}), \qquad (7)$$

where the (complex) time-dependent principal components are given by

$$A_n(t) = \sum_{\mathbf{x}} U(\mathbf{x}, t)B_n(\mathbf{x}). \qquad (8)$$

With proper normalization $\langle B_nB_m^*\rangle_{\mathbf{x}} = \delta_{nm}$ and hence $\langle A_nA_m^*\rangle_t = \lambda_n\delta_{nm}$. As in standard EOF analysis, the nth complex EOF has associated with it a fraction of

[1] See Appendix A for extension of these methods to vector fields.

the total field variance given by $\lambda_n/\Sigma\,\lambda_m$ (cf. Preisendorfer *et al.*, 1981).

Four measures that define possible moving features in $u(\mathbf{x}, t)$ can be defined immediately without assumption on the form of u. Since these measures are defined in the $\mathbf{x}/t$ domain their interpretation does not suffer as much in the presence of cyclo-stationary effects as would the interpretation of $\phi_{jk}(\omega)$. In fact, the time-dependent measures give a clear description of cyclostationary effects (if they are present). To aid the interpretation of these measures we carry along with their definitions a simple example for the case $u(\mathbf{x}, t) = a\,\sin(kx - \omega_0 t)$, i.e., a wave of constant amplitude and frequency propagating in the positive $\hat{x}$ direction.

1) Spatial phase function $\theta_n(\mathbf{x})$

This function shows the relative phase of fluctuations among the various spatial locations where u is defined. This measure, for which an arbitrary reference value must be selected, varies continuously between 0 and 2π (it is no longer restricted to 0 or π as in standard EOF analysis) and is defined by

$$\theta_n(\mathbf{x}) = \arctan\left[\frac{\mathrm{Im}B_n(\mathbf{x})}{\mathrm{Re}B_n(\mathbf{x})}\right]. \tag{9}$$

In the example cited above the data field is composed solely of a single sinusoid with wavelength L propagating along the $\hat{x}$ axis. In this case there will be only one eigenmode ($n = 1$). Then $\theta_1(\mathbf{x})$ will go through one complete cycle (2π) over a distance L measured in the $\hat{x}$ direction, i.e., $\theta_1(\mathbf{x}) = kx = 2\pi x/L$. Hence the spatial derivative of θ provides, for simple fields, a measure of the "local" (vector) wavenumber. Both Wallace (1972) and R. Davis (personal communication) suggest the difficulty of interpreting a measure like $\theta_n(\mathbf{x})$ in even moderately complex wave fields, an idea verified by theoretical calculations in this study. Such difficulty might be overcome via the filtering operation described in the Appendix. Fortunately, the principal phase information obtained in this work, *without filtering,* was simple enough in structure for easy interpretation.

2) Spatial amplitude function $S_n(\mathbf{x})$

This measure shows the spatial distribution of variability associated with each eigenmode and may be interpreted as in a normal EOF analysis. The definition is

$$S_n(\mathbf{x}) = [B_n(\mathbf{x})B_n^*(\mathbf{x})]^{1/2}. \tag{10}$$

The distribution of S gives a measure of spatial homogeneity, by mode, in the magnitude of the u-field. For the simple, constant amplitude sinusoid discussed above, S_1 = constant since a is independent of $\mathbf{x}$.

3) Temporal phase function $\phi_n(t)$

This measure describes the temporal variation of phase associated with $u(\mathbf{x}, t)$ and is given by

$$\phi_n(t) = \arctan\left[\frac{\mathrm{Im}A_n(t)}{\mathrm{Re}A_n(t)}\right]. \tag{11}$$

For the simple sinusoid with fixed frequency and wavenumber, one obtains $\phi_1(t) = \omega_0 t$ = constant $\times$ t. Hence the time derivative of ϕ is directly proportional to temporal or "instantaneous" frequency. This information does not appear to have been used in previous relaetd work, but it will turn out to provide some fascinating results in this study.

4) Temporal amplitude function $R_n(t)$

A measure of temporal variability in the magnitude of the modal structure of the u field is obtained from

$$R_n(t) = [A_n(t)A_n^*(t)]^{1/2}. \tag{12}$$

For the simple sinusoid whose amplitude does not vary with time R_1 = constant. Both $R(t)$ and $\phi(t)$ are useful in detecting cyclo-stationary processes.

The parameters defined in 1)–4) above constitute a general description of possible moving features in u. These descriptions can be further compressed by combining the spatial (temporal) amplitude and phases into vector format, e.g., $S_n e^{i\theta_n}$. Such representations are referred to here as spatial or temporal "state vectors." If the field is suitably simple, these measures can be related to common wave forms (e.g., sine wave, Kelvin wave, etc.). However, as noted above, once the complexity of the field increases beyond several propagating features of irregular form, the easy interpretations are generally no longer possible, although some useful information can still be derived from the analysis (cf. Wallace, 1972; Rasmusson *et al.*, 1981).

c. *Summary*

A complex data set (U) composed of a given real data set (u) and its Hilbert transform ($\hat{u}$) carries the equivalent of both co- and quadrature information on the temporal phase of fluctuations in u. Hence the zero lag covariance function of U can be used to investigate propagating features in u. Extraction of the eigenmodes of this covariance matrix allows one to study the largest spatially coherent "signals" present in the data set. The entire procedure is intimately linked to the estimation of a cross spectral matrix and its eigenstructure. However, the complex EOF analysis allows one to investigate easily, in space and time, the dynamic behavior of energetic events or cyclostationary processes. Such features might well be obscured in the normal spectral analysis approach.

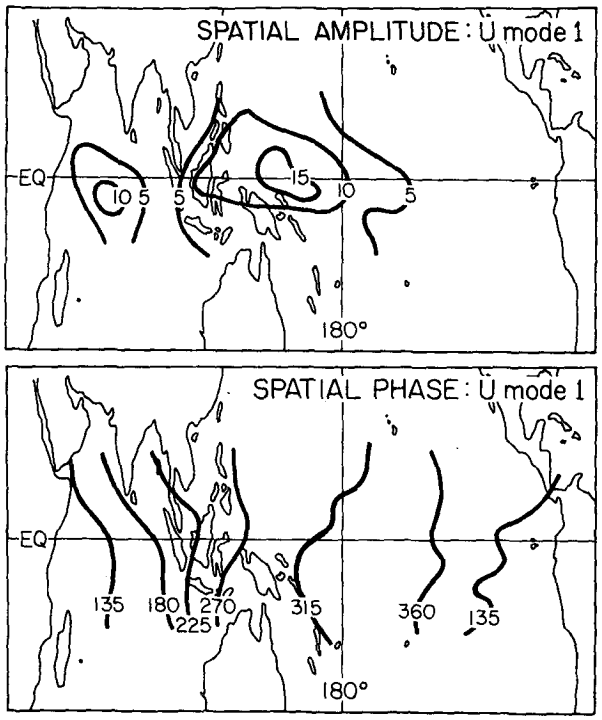

FIG. 3. The spatial amplitude (upper, relative units) and relative phase (lower, degrees) for mode 1 of the zonal component analysis.

4. Zonal flow: Walker cell

The zonal component of the anomalous wind field was analyzed according to the methods of Section 3. The EOF dominant variance filtering rules of Preisendorfer *et al.* (1981) suggest the first 10 eigenmodes were distinguishable from those expected from a white noise process. This means 43% of the variance contained in the u-component of the Monsoon/Trade Winds field can be classified as "signal," the rest being attributed to "noise." Discussion will be limited to the first two modes which account for 38% of the non-noise variance, and appear to be "distinct" (cf. North *et al.*, 1982). The discussion is relevant to the properties of the Walker cell if one assumes that cell is bound by latitude 10°.

a. Spatial properties

The spatial amplitude and relative phase for mode 1 are shown in Fig. 3 and their zonal and meridional averages in Figs. 4 and 5. The following conclusions were drawn from these illustrations:

1) The largest variability in the zonal component occurs west of the dateline in the confluence region of the Monsoon and Trade Winds. A secondary maximum exists in the central Indian Ocean. This mode contains 27% of the non-noise field variance. Fig. 5 shows this variability to be symmetric about the equator and to have its maximum energy there also. The second eigenmode (13% of the signal) has multiple maxima in much the same regions noted above. However, the energy distribution has a clear minimum at the equator and a skewing toward the South Pacific Convergence Zone (SPCZ) off the east coast of Australia. Neither the first or second eigenmode show appreciable energy in the eastern equatorial Pacific.

2) The distribution of phase associated with mode 1 increases in a nearly linear fashion to the east. The first-order interpretation suggests propagation of anomalies from the Indian Ocean to the western Pacific (Fig. 3, lower; Fig. 4, simple example Section 3b). Since the phase is essentially the same on either side of the equator (Fig. 5) the direction of propagation is easterly to within ±30°. *Thus the perturbations in zonal flow (Walker Cell) appear first in the Monsoon and later manifest themselves in the Trade Winds.* Note Fig. 3 (upper) suggests an intensification of these anomalies as they cross Indonesia and enter the Pacific. Their motion can be followed to 140°W although they attenuated rapidly east of the dateline. The slope of $\theta_1(\mathbf{x})$ in Fig. 4 suggests a wavelength roughly corresponding to planetary wavenumber 2.

The propagating feature seen in Figs. 3 and 4 is slightly more complex than a simple sinusoid. This is seen in the dual energy maxima (70°E, 170°E), energy minimum (90°E), and non-uniform increase in phase around the longitude of the energy minimum. Simple theoretical considerations and numerical simulations show that the spatial distribution of amplitude/phase shown in Figs. 3 and 4 can be explained as the linear superposition of an eastward propagating wave and a standing wave. Such a feature will have nearly all of its energy picked up by a single complex eigenmode. The requirements on these waves necessary to reproduce the observed pattern are that (i) their amplitudes be nearly equal (This appears to be an important constraint.) and (ii) their wavenumbers be roughly equal. The results of Section 4b also suggest their frequencies are nearly equal.

b. Temporal properties

The time-dependent amplitude and phase are shown for mode 1 in Fig. 6 along with the temporal state vector and SST anomaly at Talara, Peru. These results lead to the following conclusions:

1) The temporal amplitude function clearly shows the increase in anomalous zonal flow between 1970–76 compared to the earlier two decades. It may be noted also that the relative peaks in $R_1(t)$ more or less match major El Niño events, although this correspondence is not exact.

2) The temporal phase $\phi_1(t)$ exhibits a relatively well behaved linear trend over any 2π interval, except perhaps during 1967 when the temporal amplitude function is low and the mode 1 pattern almost non-

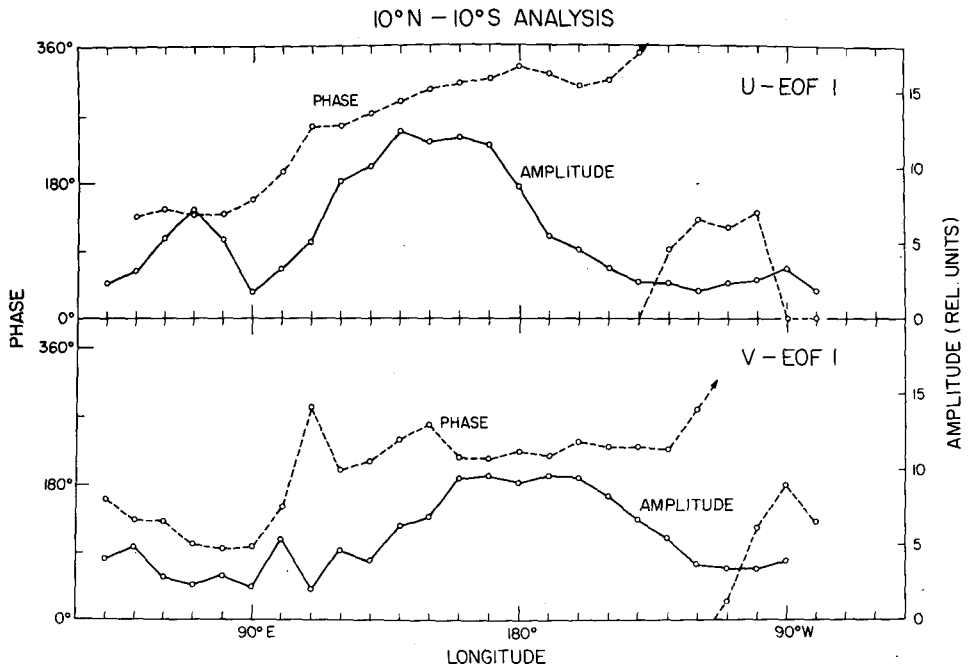

FIG. 4. Meridional average of spatial phase and amplitude for mode 1 of the u and v component of the combined Monsoon/Trade Wind field.

existent in the basic data set. Also the temporal state vector ("STICK") exhibits a semiregular counterclockwise rotation. These facts suggest a quasi-periodicity for mode 1 behavior. In fact, $\phi_1(t)$, when plotted as a continuous function, was well represented over the period 1953–78 as the argument for a fre-

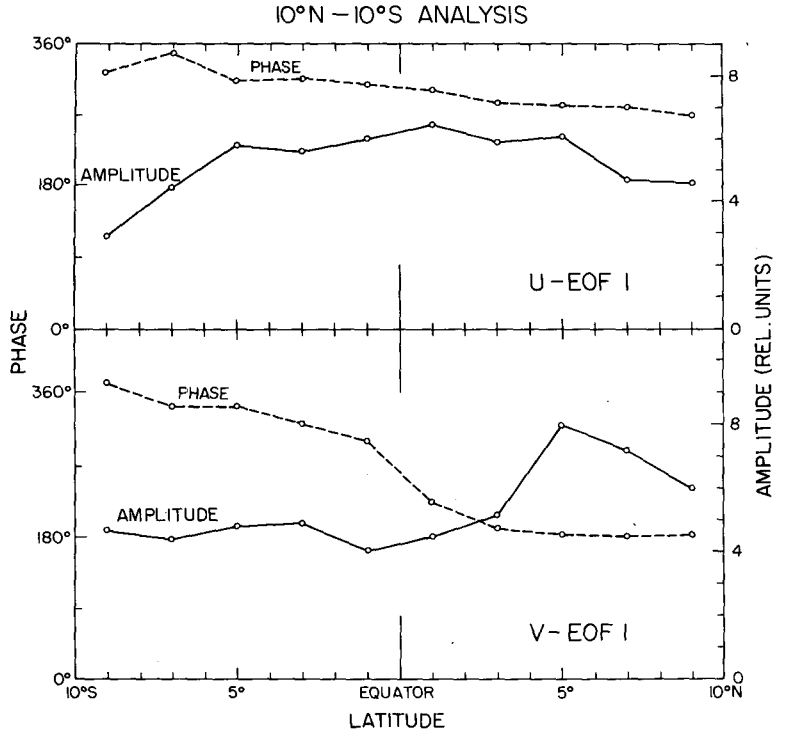

FIG. 5. Zonal average of spatial phase and amplitude for mode 1 of the u and v component of the combined Monsoon/Trade Wind field.

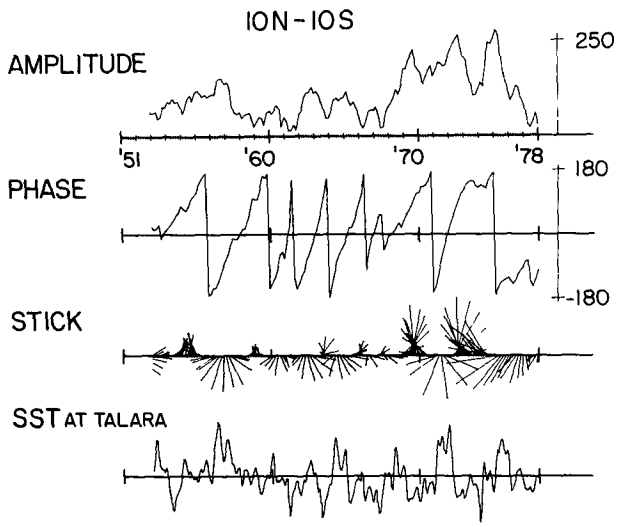

FIG. 6. Temporal properties from the complex EOF analysis of the u component of the Monsoon/Trade Wind fields. Upper panel: amplitude function; second panel: phase; third panel: state vector; bottom panel: sea-surface temperature anomaly at Talara, Peru. The information shown on the first three panels has been smoothed with a five-point running mean filter. The last panel has been smoothed with a three-point Hanning filter.

quency-modulated wave (Fig. 7) of the form $\phi_1(t) = \omega_0 t + A \sin\omega_1 t$. The fundamental period ω_0 was 3.3 years and modulation period (ω_1) was roughly 25 years; only one realization of the modulation exists in the data set. This apparently poorly determined relation has some surprising consequences as we shall see in Part III.

3) A detailed study of the unsmoothed $\phi_1(t)$ shows them to be locked to the seasonal cycle. Values of π occur in the September–December time frame in 4 out of 7 cases, with the three remaining cases occurring in late spring. The feature of the wind field captured in mode 1 is therefore cyclostationary. The lower panel of Fig. 6 shows that ϕ_1 attains values of π typically 2–6 months *prior* to anomalous increases in SST at Talara, Peru. This happens for every warming event over the period 1953–78, except during the 1967–69 period. Features 2) and 3) and their relation to El Niño events will be discussed further in Part III.

4) The temporal behavior of mode 2 is less regular than mode 1 suggesting the absence of highly organized information. The one exception to this statement is the rather clear appearance of an apparent quasi-biennial oscillation in $R_2(t)$ between 1960–78. This feature did not appear in $\phi_2(t)$, which resembles a low-frequency random process. The biennial properties of the Monsoon/Trade Winds appear more clearly in the vector analysis and will thus be discussed in Section 6.

c. *Reconstructed flow field*

The features of the zonal flow discussed above can be brought to life through a partial field reconstruction according to Eq. (7). The large El Niño event of 1972 is a convenient marker for these reconstructions. *None of the features noted below are unique to that particular event* although they do have larger than average amplitude in that year (1976 and 1958 also).

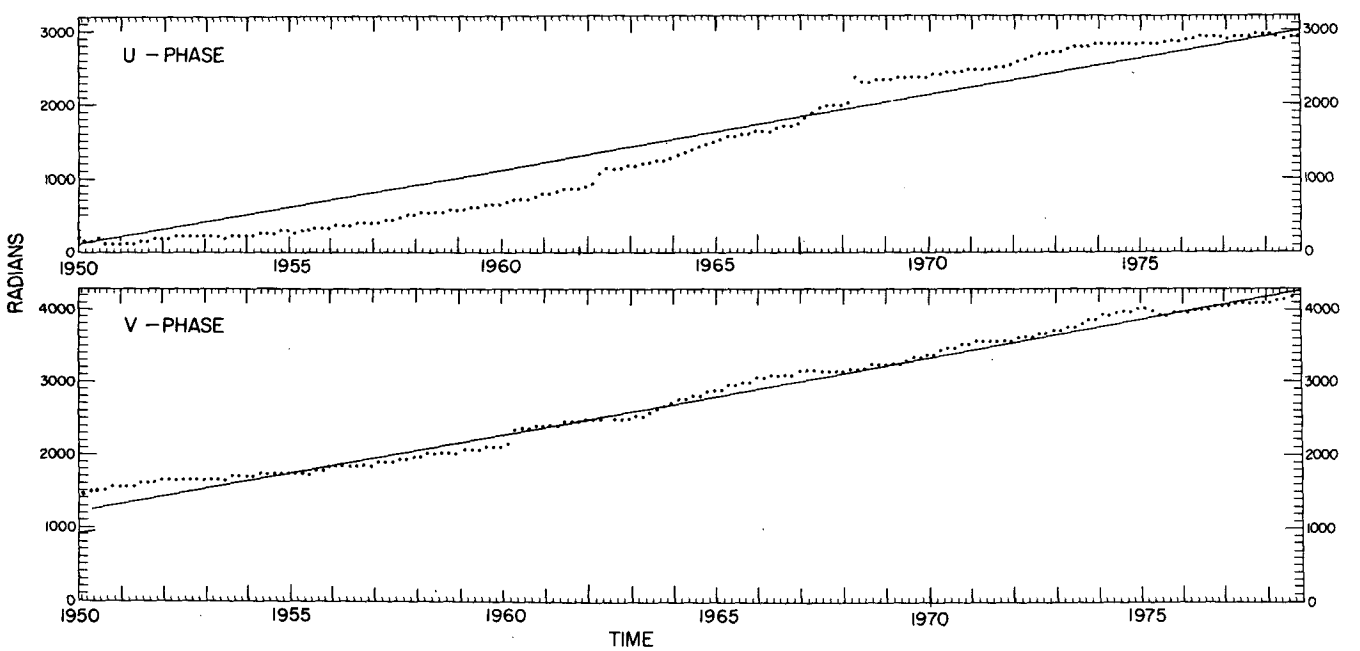

FIG. 7. Phase from the u and v component component analysis shown as continuous functions of time. If the oscillations in these fields were pure sinusoids then all of the data points (dots) would lie along the best-fit straight line.

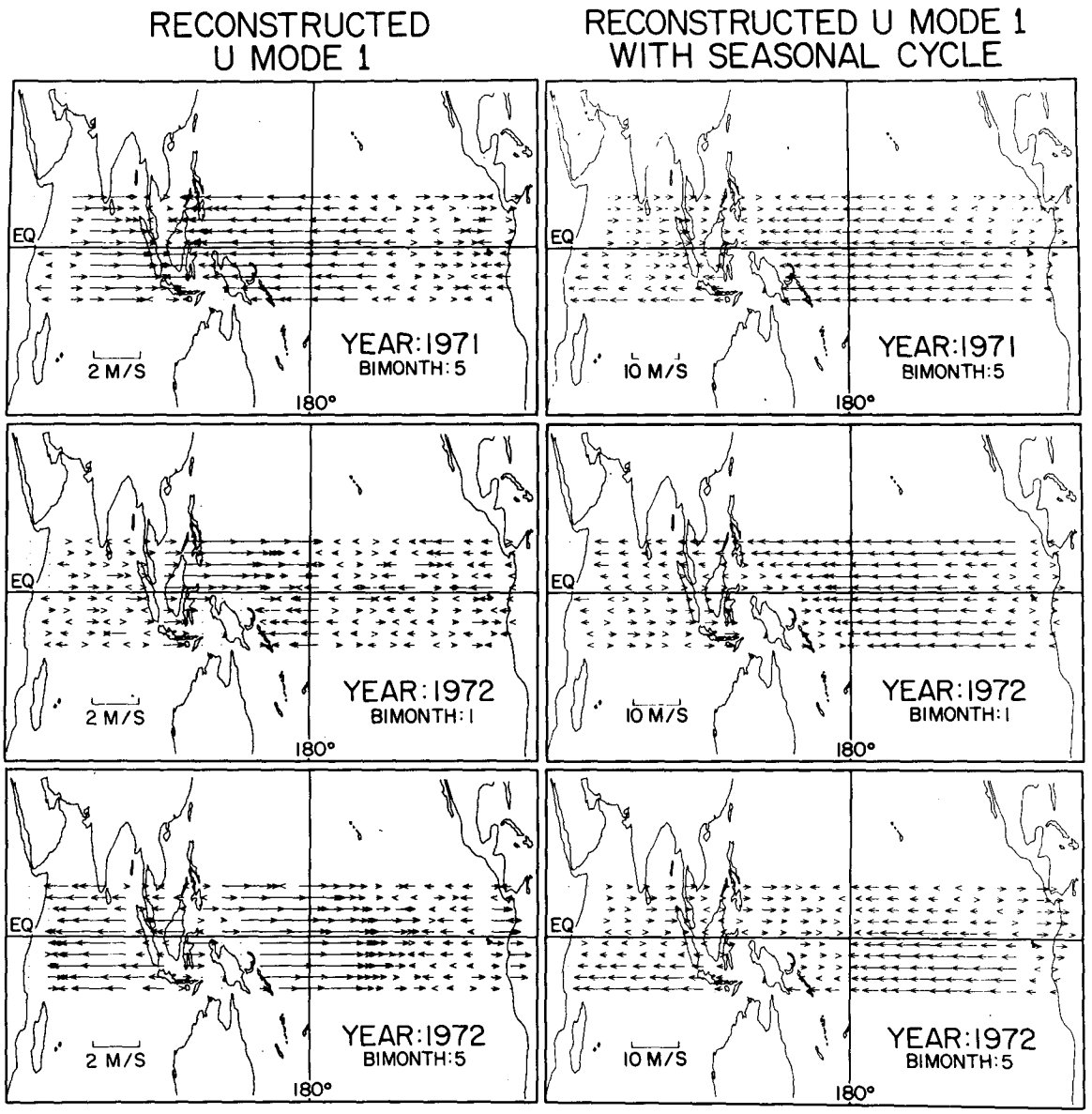

FIG. 8. Reconstructions of the zonal anomaly field associated with mode 1. Upper panel: left, reconstructed anomaly field during September and October 1971; right, anomaly field plus seasonal cycle; middle panel: reconstructed field for January–February 1972; lower panel: reconstructed field for September–October 1972. These reconstructions correspond to the two quasi-stable states and transition state in the Monsoon/Trade Winds system.

Fig. 8 shows the resultant anomaly fields (mode 1) plus the combined anomaly/season cycle fields.

The upper panel shows the strong anomalous convergence in the zonal flow field over Indonesia during the late summer/early fall of 1971 and corresponds to stronger than normal summer Monsoon plus westward extension of the Trade Winds system. A weak divergence exists in the eastern Pacific. Addition of the seasonal signal (upper right) moves the actual convergence slightly east from Indonesia and confines the Walker cell to the region 10°N–5°S. The idea of a cell symmetric about the equator is too simple to describe the additional complexity introduced by the seasonal signal. These upper panel illustrations are typical of cold equatorial SST's in the eastern Pacific and one phase of the standing wave/progressive wave pattern noted in Section 4a.

The middle panels show one aspect of the wind field transition that *precedes* oceanic warming at South America. The convergence over Indonesia weakens due to the failure of the northeasterlies to penetrate as far west as usual (weak winter monsoon). Addition of the seasonal signal shows the main zonal convergence area to lie east of its normal position

with a complicated divergence system over both the Indian and eastern Pacific Oceans. The eastward motion of the main convergence from Indonesia was the propagating feature detected by the spatial phase function (Section 4a). Again, the concept of a simple symmetric Walker cell seems inadequate to describe the middle panels.

The lower panels represent late summer/early fall conditions during the height of the 1972 El Niño. A strong anomalous zonal divergence exists over Indonesia and convergence east of the dateline. This result is due to an eastward retreat of the Trade Winds and weak Summer Monsoon in the Indian Ocean. Addition of the seasonal signal, however, *suggests that the Monsoon System can be thought of as displaced north and east of its normal domain.* Indeed, eastward flow exists to the dateline. The main zonal convergence zone has been displaced to the dateline and so the node of the Walker Cell has been similarly displaced from its normal position, a situation also noted by Trenberth (1976) and others. The eastern node off South America remains essentially in place so the western branch of the cell lengthens at the expense of the eastern branch. Note also the change in character of the zonal convergence in the Indian Ocean and the strong asymmetric flow about the equator. These features are strongly related to SST and rainfall patterns as will be discussed in Part III.

5. Meridional flow: Hadley cells

The meridional component of the anomalous wind field was analyzed according to the methods of Section 3. The EOF signal/noise separation techniques suggest the first 10 eigenmodes were distinguishable from a white noise process. Discussion will be limited to the first two modes which together account for 46% of the "signal," and are "distinct." The discussion gives a partial view of the behavior of the hypothetical Hadley cell. Part II covering the region ±30° of the equator will give a more complete description.

a. Spatial properties

The interesting spatial features of the v-field are summarized below.

1) The maximum energy in the first mode (30% of the signal) of the v-field is centered near the dateline (Fig. 4) and hence associated principally with the Trade Winds. This represents a shift of roughly 40° of longitude from the most energetic region of the u-field. Maximum variability occurs on average near 5°N with a minimum at equator and a weak secondary maximum near 3–5°S. The meridionally averaged phase values resemble those expected of a standing wave pattern except perhaps east of the dateline where west-to-east transfer of information is suggested.

2) Fig. 5 shows the meridional components in the two hemispheres are 90–180° out of phase and suggests either propagation of information from north to south across the equator or an approximate standing wave pattern between the hemispheres. The highest variability is near 5°N with a poorly defined minimum at the equator.

Detailed examination of θ_1 field (not shown) leads to a more complex pattern than the simple one described above. The anomalies appear first in the southeastern Indian Ocean and SPCZ region at 10°S, the southern limit of the current analysis. The anomalies quickly spread over the entire Indian Ocean. Perturbations appear in the eastern Pacific between 3–10°N coincident with this spreading. In the Northern Hemisphere, the perturbations move east from the Indian Ocean and west from South America, merging near 150°E. Zonal motion in the anomaly field is hard to discern in the Southern Hemisphere. The meridional anomalies averaged over the oceans (Fig. 4) are roughly 180° out of phase (standing wave).

3) Mode 2 non-noise variance (16%) was confined largely to the Monsoon region of the Indian Ocean, particularly along the coast of Africa, and to the coastal regions off South America. The fluctuations in these regions were all in phase, essentially synchronous. In fact, the variations represented by this mode were in phase over virtually the entire equatorial region from Africa to South America. It appears that both the Monsoon and Trade Winds share a common mode of variability that is associated with spatial scales longer than both fields themselves.

b. Temporal properties

The v-component (mode 1) displays very definite temporal characteristics (Fig. 9). This illustration shows:

1) Mode 1 has a relative maximum in amplitude associated with every El Niño event since 1953. These maxima occur late in the El Niño cycle when anomalously warm water is in the central Pacific. Note that these maxima *lag* the phase transitions seen in the u-field (Section 4b) by roughly 9–12 months.

2) The temporal phase $\phi_1(t)$ obtains a value near 0° that is tightly phase-locked to the annual cycle and occurs in the late Northern Hemisphere fall, again during the most intense phase of the El Niño in the central ocean. It will be shown in Part III that $\phi_1 = 0°$ corresponds to the transition between anomalous meridional convergence/divergence over the Indonesian area.

3) The behavior of ϕ_1 is quasi-linear over intervals of 2π suggesting mode 1 can be characterized as a quasi-periodic event, although the years 1959 and 1975 disrupt this pattern. The continuous representation of θ_1 (Fig. 7) again weakly suggests a frequency-

modulated process. Further discussion of this possibility is deferred to Part III.

4) The temporal behavior of mode 2 was highly unusual. Prior to 1960 and after 1976, $R_2(t)$ varied randomly and $\phi_2(t)$ showed a slow monotonic rise associated with a frequency of roughly 1 cycle per 20 years. Between 1961–76, however, $R_2(t)$ showed a rather well-defined biennial oscillation with average period 26 months. The temporal phase over this period shows abrupt increase in slope corresponding to roughly 1 cycle per 4 years. It was noted in Section 5a that this fluctuation was coherent over both the Monsoon and Trade Winds. We will return to the biennial characteristics of the record in Section 6 and Part III.

c. *Reconstructed flow field*

The anomalous v-field associated with mode 1 was reconstructed and is shown in Fig. 10 along with the combined anomaly/seasonal cycle field. The reconstruction periods are the same as those selected for the u-field.

The strong Monsoon-expanded Trade Winds situation (upper panels) is marked by anomalous flow from the Northern to the Southern Hemisphere over the Indian Ocean. Apparently the Monsoon is somewhat more zonally directed than normal. In the central and Indo-Pacific the anomalous cross-equatorial flow is in the opposite sense—from south to north. Note that in both wind systems the anomalies are a significant fraction (or larger than) the seasonal signal itself, except in the eastern Pacific. Inclusion of the seasonal signal shows interhemispheric near-surface transfer of mass from south to north over the entire Monsoon/Trade Winds system (is there a compensating flow at upper levels?).

During the transition period (January–February 1972) when the zonal anomaly is moving into the Indo-Pacific, the anomalous meridional field is largely unchanged. This is seen pictorially in Fig. 10 plus shown in the amplitude/phase values given in Fig. 9.

During the time of unusual warmth in the central Pacific (lower panels), the anomalous north-to-south flow over the Indian Ocean has intensified as the zonal component of the Monsoon weakened. The major change in the v-component, however occurs in the central Pacific where the anomalies suggest intensified convergence over virtually the entire Trade Winds system near the equator. Addition of the seasonal signal shows the ITCZ east of the dateline has shifted southward (see also Weare, 1981). Increased convergence also is suggested in the Indo-Pacific. The result of these changes should be a redistribution of rainfall in the equatorial band, a familiar result discussed in Part III (see also Berlage, 1966; Bjerknes, 1966; Rasmusson and Carpenter, 1982; among others).

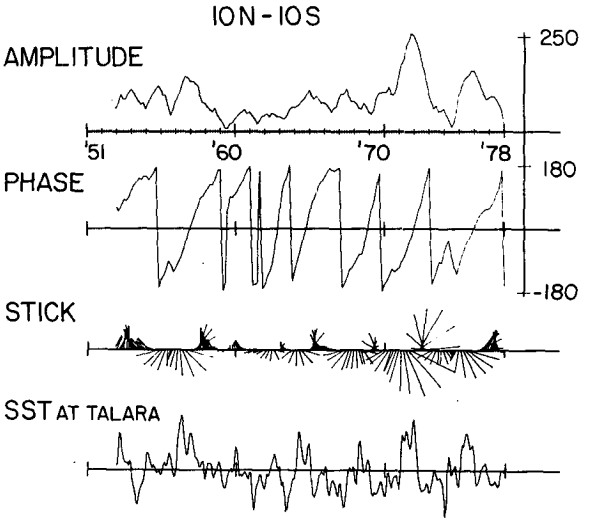

FIG. 9. Time-dependent amplitude, phase and state vector for anomalous v component of the Monsoon/Trade Wind fields, mode 1, and SST at Talara, Peru (see Fig. 6 legend).

6. Vector field

The (u, v) components were combined according to (A7) and the resulting field analyzed by the methods of Section 3. Computer limitations required use of a $2° \times 20°$ grid. However, the $2 \times 10°$ grid will be retained for display purposes. The EOF filtering suggested 45% of the variance in this vector field could be considered signal.

a. *Spatial amplitude and phase*

The spatial state vector described in Section 3b was estimated using the composite phase given in (A9). The results are filtered to eliminate weaker signals and displayed in Fig. 11. The following conclusions were drawn from this illustration.

1) The composite phase (Fig. 11, upper) suggests there are essentially three coherent regions of variability for mode 1 (24% of the signal). The eastern Pacific, north of the equator and the western Indian Ocean (hereafter called Region 1) fluctuate in unison since these phases are roughly 90–120°. The close coupling of the Monsoon/Trade Winds is again demonstrated. The area around Australia and the SPCZ (Region 2) shows coherent variation that is approximately 180° out of phase with Region 1. Finally the region of the Northern Hemisphere maritime continent (Region 3) is coherent but lags Region 1 by about 90°. The variations of phase *within* Regions 2 and 3, where the largest magnitude signal occurs, is suggestive of west-to-east transfer of information although this feature is not as strong as in the analysis of the zonal component alone.

2) Maximum amplitude for mode 2 (16%), as shown by the 3–4 barbs, occurs in the western Indian

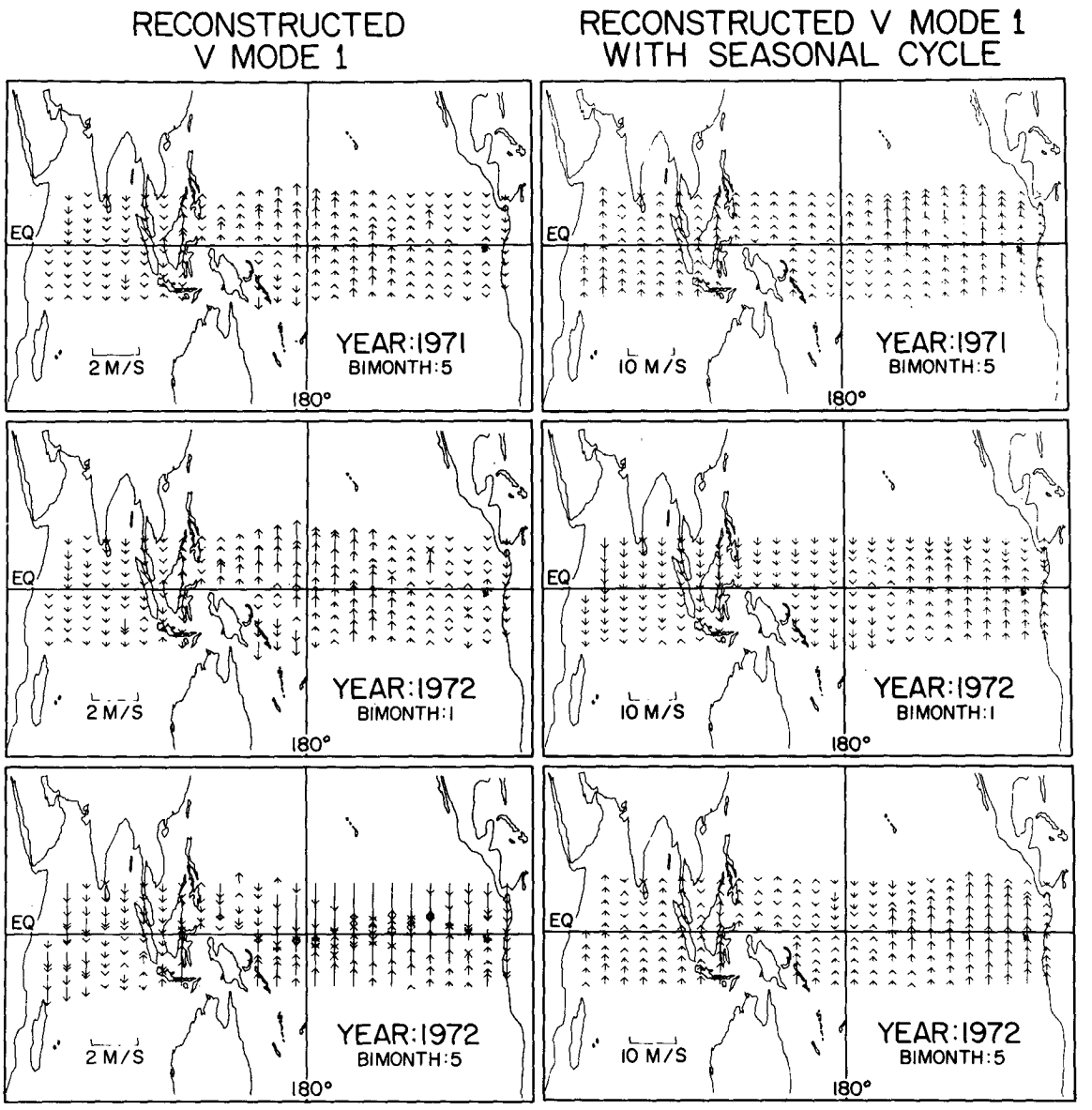

FIG. 10. Reconstructions of the meridional anomaly field associated with mode 1. Upper panel: left, reconstructed anomaly field during September and October 1971; right, anomaly field plus seasonal cycle; middle panel: reconstructed fields for January–February 1972; lower panel: reconstructed fields for September–October 1972. These reconstructions correspond to the two quasi-stable states and transition state in the Monsoon/Trade Winds.

Ocean, north of the equator, and immediately along the coast of South America (Fig. 11, lower). The sense of the mode 2 phasing suggests a standing wave pattern. The flow in the Indian Ocean and the area off South America are approximately in phase. The maritime continent and area of the date-line, although possessed of weak signal strength, are essentially 180° out of phase with these two areas. Close inspection of the u, v components separately shows this result is largely determined by the properties of the meridional flow field since the direction of zonal flow anomalies is almost perfectly asymmetric about respect to the equator.

b. Temporal amplitude and phase

These measures of variability provide fascinating and unexpected results for both the vector modes discussed above. The appropriate information is shown in Figs. 12 and 13.

1) The temporal state vector (STICK) for mode 1 exists in an *apparently* bimodal state. The two states are 180° out of phase with each other. Let us denote these two states by the letters C and W, depending on whether the SST in the eastern equatorial Pacific is colder or warmer than usual. Close inspection of

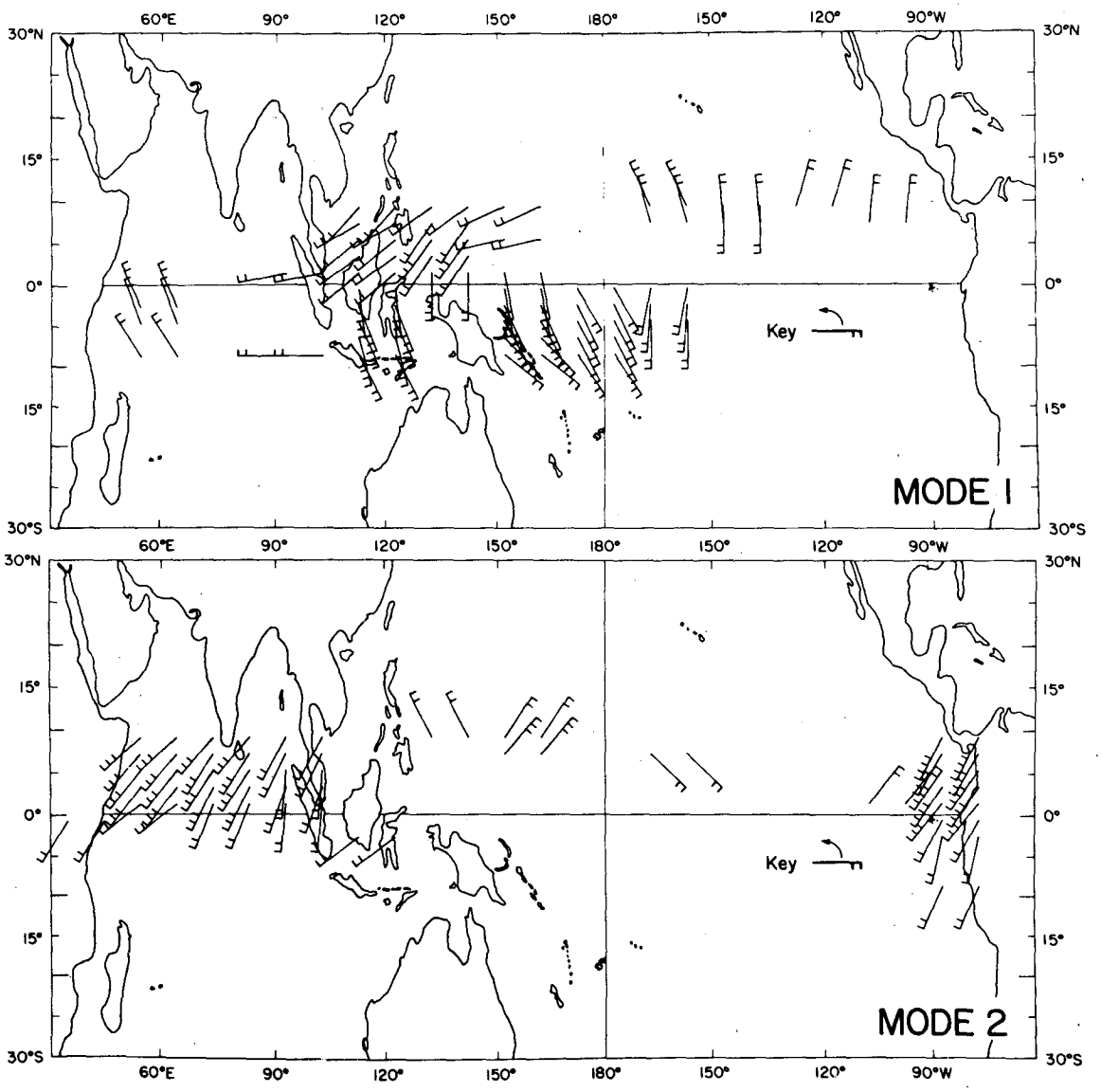

FIG. 11. Spatial state vector of the anomalous vector component of the Monsoon/Trade Winds system. The number of flags indicate the magnitude of spatial power (in relative units of 0.05). Signals < 0.10 have been omitted. The direction of the flag indicates the relative spatial phase of fluctuations in different regions of the field. Phase is measured counterclockwise with respect to the positive, x axis (see key in lower right-hand corner). Upper panel: results from mode 1 analysis; lower panel: results from mode 2 analysis.

the PHASE curve (Fig. 12) shows the bimodal behavior is only partially true. Upon obtaining a mean value for a given state, say C, the phase slowly drifts higher until it reaches some treshold value. At that point a rapid transition to the other preferred state (W) occurs and the same process repeats itself with a subsequent shift to C. The residence time in each state can be years, although the wind system exhibits a longer dwell time in C than it does in W. Note the transition between states occurs rapidly compared to the time spent in either state.

2) The temporal behavior of mode 2 is somewhat discontinuous. Between 1954–72, $R_2(t)$ shows a marked quasi-biennial oscillation (QBO) with average period 26 months. During this period, $\phi_2(t)$ suggests irregular, instantaneous frequencies of order 1 cycle per 20–40 months. In the earlier years, when the data are sparse, R_2 is irregular and ϕ_2 shows a slow trend of order 1 cycle per 6–8 years. After the early 1970's the interannual change in the seasonal cycle (Section 2b) affects the analysis. It appears that there is a QBO-like signature in the Trade Winds/Monsoon and that this signal could be characterized as an amplitude-modulated process riding a quasi-random, but low-frequency, carrier. However, the signal is rather discontinuous appearing to "turn-on" and "turn-off" in the space of a single cycle. It may persist, however, for the order of a decade.

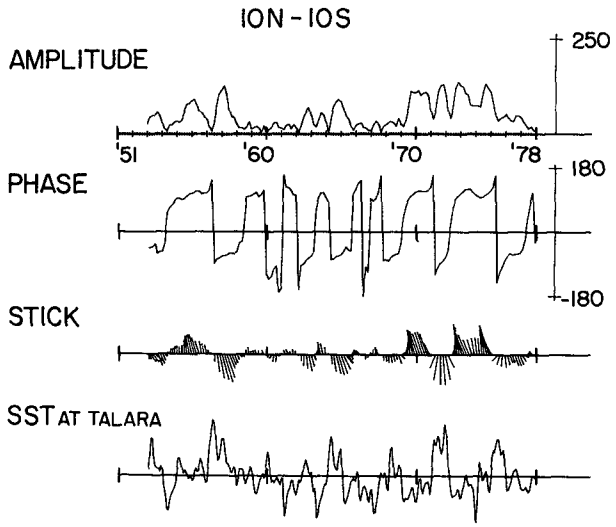

FIG. 12. Time-dependent amplitude, phase and state vector for the anomalous vector component of the Monsoon/Trade Winds, mode 1, and SST at Talara, Peru (see Fig. 6 legend).

c. *Reconstructed flow field*

The reconstructed anomalous flow fields for mode 1 that go with states C and W are shown in Fig. 14. The upper panel (C) shows usually strong convergence over Indonesia with the largest anomalous convergence in the Northern Hemisphere and a secondary maximum northwest of Australia. Note that this reconstruction shows the principal feature seen in the raw data field for the same bimonth and year (Fig. 2). The reconstructed pattern results from the facts that 1) the Monsoon has intensified but goes no further east than Sumatra, and 2) the easterlies expanded into the western Pacific (upper left panel). There is anomalous divergence above the equator in the eastern Pacific but this is overwhelmed by the stronger seasonal cycle so the southeasterlies penetrate across the equator to nearly 140°E.

During the transition from C to W the anomalous convergence over Indonesia weakens (Fig. 14, middle). More important, the center of the anomalous convergence shifts toward New Guinea. This coincides with a weakening of the winter monsoon in the Northern Hemisphere and the establishment of a strong convergence zone directed northwest–southeast from the South Pacific into the Indo-Pacific. Both the Monsoon/Trade Winds in the Southern Hemisphere near the equator remain anomalously strong. The main point here is that the weakening appears first in the Northern Hemisphere. Part II will suggest a Southern Hemisphere anomaly source in addition.

During state W (Fig. 14, lower), the region of largest convergence has shifted to and broadened about the equator, while the region over Indonesia experiences a reduced convergence (anomalous divergence). This flow pattern is associated with weakened Monsoon over the northern Indian Ocean and truncation of the easterlies west of the dateline. Between the dateline and Indonesia the flow, *both* anomalous and absolute, is now eastward. This reversal of direction could be considered an expansion of the Monsoon system into the western Pacific, a phenomena also suggested to occur by Ding and Reiter (1981). These features are similar to those discussed in Section 4c but then the vector anomalies are driven principally by the zonal component [$R_{uv} = 2$; Eq. (A8)].

The patterns shown above represent a pulsation and spatial translation of the Indonesian convergence on a massive scale. The anomaly patterns *appeared* bimodal (Section 6b) since they represented convergence or divergence, processes that are by definition 180° out of phase (Fig. 12). Addition of the seasonal signal shows the actual flow field to be always convergent over Indonesia. It is the magnitude of this convergence and the area it covers that are modulated. However, the position of the most intense convergence shifts eastward some 40° of longitude during W events. Note the maximum anomalies, or anomalous convergence, is east of the date line—some 30–40° east of the actual convergence maximum. The eastward drift of the actual convergence appears to take some months. The reversal to C is a more rapid process that is generally accomplished in 1–2 bimonths (see Section 7).

7. Conclusion

A time history of Monsoon Systems (Monsoon) over the Indian Ocean from 1947–78 has been constructed and merged with a comparable history of the Pacific Trade Wind Field (Trade Winds). A rather new analysis technique has been applied to a subset of this merged data set covering the region ±10° of the equator, extending from Africa to South America

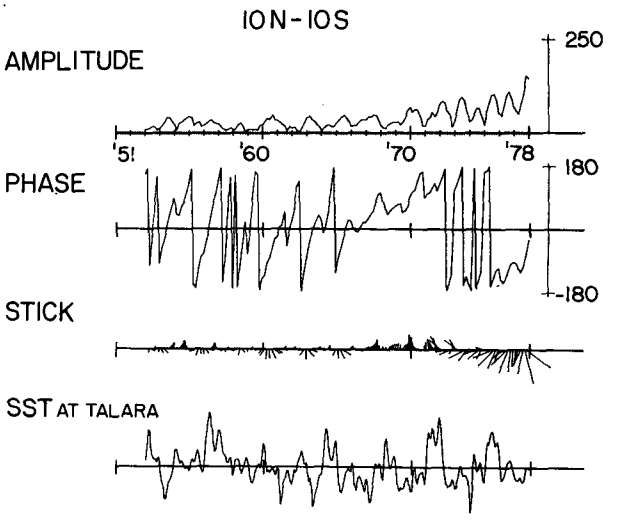

FIG. 13. As in Fig. 12 except for mode 2.

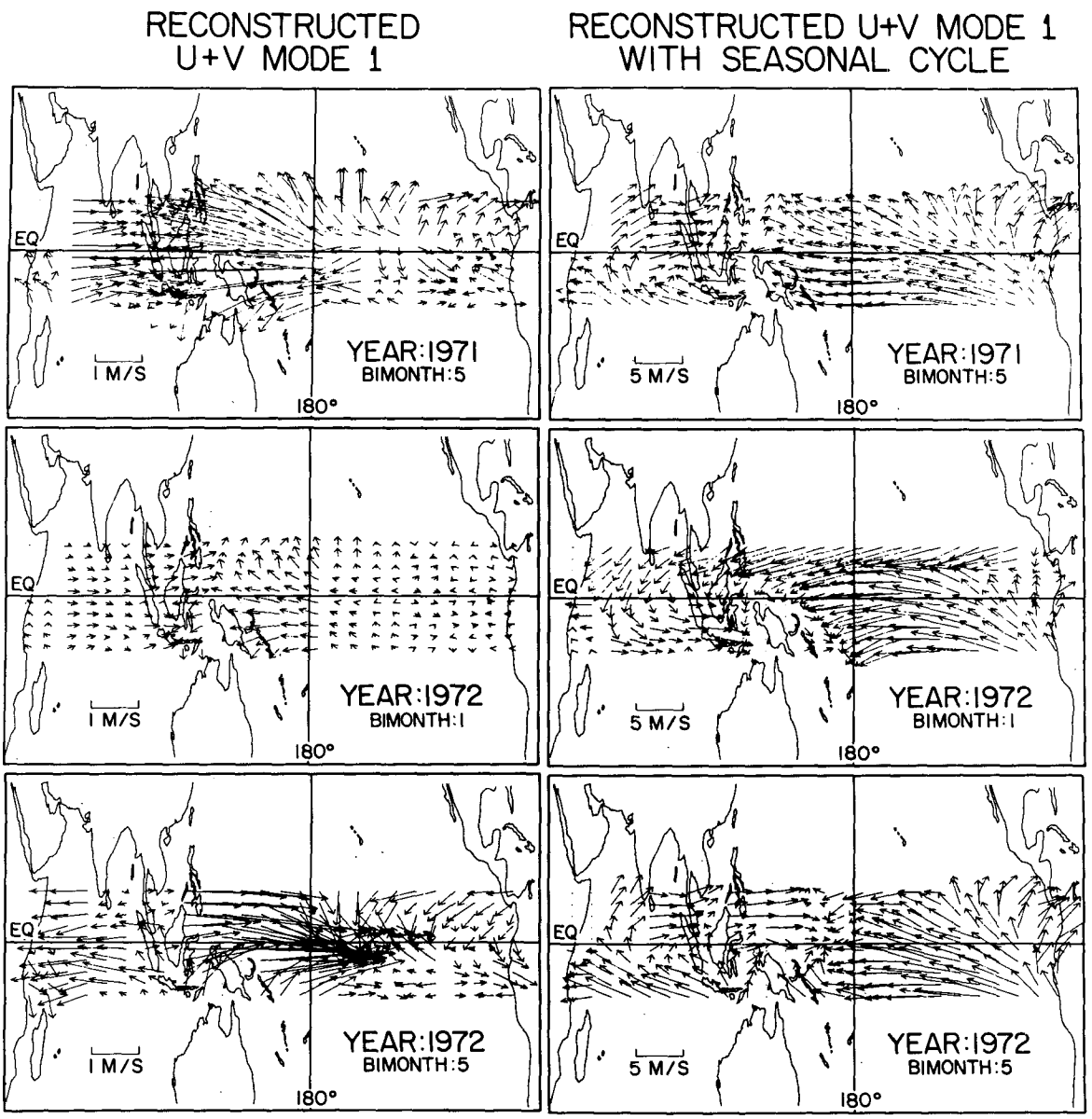

FIG. 14. Reconstructed anomalous vector field associated with mode 1. Upper panel: anomalous winds of the Monsoon/Trade Winds field associated with state C (September/October, 1971); middle panel: wind field during the transition from state C to state W (January/February, 1972); lower panel: anomalous wind field associated with state W (September/October, 1972). The left portion of each panel is associated with the anomalous flow field. The right portion of each panel is a combination of the anomalous flow plus the normal seasonal cycle.

over the time interval 1952–78. The analysis method is designed to locate regions of spatially large covariability and to detect the presence (or absence) of propagating features in the data field. The method largely avoids problems of nonstationarity arising from event-like features and cyclo-stationarity.

The principal results of this part of the study, which concentrated solely on the description of the space/time character of the field noted above, are as follows:

1) The Monsoon and Trade Winds are strongly coupled at interannual time scales. The coupling is accomplished through pulsations of the massive low-level convergence in the Indo-Pacific created by the joint action of each wind system. These pulsations can be thought of in two complementary ways: The areal extents of the Monsoon and Trade Winds expand and contract in antiphase, i.e., the summer Monsoon extends into the Pacific nearly to the dateline while the Trade Winds retreat eastward to the dateline. These expansions/contractions are also associated with strengthening/weakening, respectively, of the individual wind systems. Alternatively one

could say the Indo-Pacific convergence shifts longitudinally some 40° of longitude while expanding/contracting its areal region of influence. These shifts are strongly related to subsequent occurrences of equatorial SST anomalies in the central and eastern Pacific (El Niño).

2) The temporal behavior of the vector wind anomalies suggests the existence of two states in the Indo-Pacific convergence system, one associated with anomalously strong convergence over Indonesia (C); the other with the maximum convergence near the dateline (W). These states may exist for periods of 1–3 years. However, while in one state, say C, there is a slow drift toward the opposite state W. The transition from C to W occurs rapidly relative to the dwell time in a given state.

3) The precursors to the large-scale changes noted above seem to be in the zonal component of the wind. This component is largely responsible for the patterns noted above. The linear superposition of a simple propagating wave-like feature and a geographically fixed standing wave pattern can explain most of the numerical results obtained by the EOF analysis. Physically, perturbations first appear in the zonal component in the Monsoon over the northern Indian Ocean, and then migrate eastward and intensify until they reach the data line, where they stall and eventually die. This result can be interpreted physically as the east/west translation of the Indo-Pacific node of the standing wave-like Walker cell. It will be shown in Part III that the propagating perturbations have nearly all of the characteristics that theory attributes to equatorially trapped Kelvin waves.

4) The meridional component, due to the geographic limitations imposed in this study, only partially represents fluctuations in the Hadley cell. Nevertheless, state C noted above is associated with an anomalous surface transfer of mass from the Southern to Northern Hemisphere. State W is characterized by a strengthening and equatorward shifting of the meridional convergence over the entire central and eastern Pacific.

5) The features noted above are phase-locked to the annual cycle, a fact readily demonstrated by other analyses (e.g., Barnett, 1981). Further, it is noted here that the behavior of the features in time is quasi-periodic, e.g., like a frequency-modulated process. This point will be taken up in Part III.

6) Mode 2 EOF patterns were discussed briefly. The common feature of these secondary patterns was that they all suggested an apparent QBO signal in the Monsoon/Trade Winds fields off the East Coast of Africa and the West Coast of South America. The signals in these regions were in phase. A weak secondary signal in the Indo-Pacific area was evident. The unanimous behavior of the second modes suggest they may represent a real pattern of variability. If so, such a pattern would suggest a standing wave behavior for the QBO in the Monsoon/Trade Winds System.

Part II will consider the behavior of the full Monsoon/Trade Winds within ±30° of the equator. Part III will synthesize the results of Parts I and II into a physical picture of the air/sea interaction in the tropical region.

Acknowledgments. Sincere thanks are due particularly to Bob Long, and also Rudy Preisendorfer, Leonid Volfson, Mark Johnson and Russ Davis for useful discussion over the course of this study. The author is also grateful to Doug Luther and an anonymous reviewer for several thought-provoking discussions/comments on the interpretations of Section 4a. Volfson carried out the calculations and produced the excellent graphics. Grace Johnston transcribed the manuscript. The computer work on that aspect of the problem was carried out by Tony Tubbs and Peter Crill. The author gratefully acknowledges the support of the Climate Dynamics Office of the National Science Foundation (Grant ATM-7918206).

APPENDIX

Work Notes on Hilbert Transforms and Complex EOF Analysis

1. Practical estimation of the Hilbert transform

There are several ways to estimate the Hilbert transform $\hat{u}(t)$ from its (real) transform partner $u(t)$. These are discussed briefly below.

a. Fourier method

In Section 3 we saw

$$u(t) = \sum_{\omega} [a(\omega)\cos\omega t + b(\omega)\sin\omega t], \qquad \text{(A1)}$$

where

$$\left.\begin{aligned} a(\omega) &= \frac{1}{T}\int_0^T u(t)\cos\omega t dt \\ b(\omega) &= \frac{1}{T}\int_0^T u(t)\sin\omega t dt \end{aligned}\right\}. \qquad \text{(A2)}$$

Since

$$\hat{u}(t) = \sum_{\omega} [b(\omega)\cos\omega t - a(\omega)\sin\omega t], \qquad \text{(A3)}$$

one may obtain $\hat{u}$ directly from the Fourier coefficients (A2) subject to the limitations of the next section. This approach will be subject to all the problems that normally attend Fourier analysis, e.g., end effects, leakage, etc. (cf. Jenkins and Watts, 1968; Bergland, 1969).

b. Convolution method

The estimate of $\hat{u}$ used in this study was obtained by performing a filtering operation on u itself. Eq.

(4) may be rewritten in the form of a convolution as

$$\hat{u}(t) = \sum_{l=-L}^{L} u(t-l)h(l). \tag{A4}$$

A simple, but adequate, filter than has the desired properties of approximate unit amplitude response and $\pi/2$ phase shift is given by Oppenheimer and Schäfer (1975) as

$$h(l) = \begin{cases} \dfrac{2}{l\pi}\sin^2(\pi l/2), & l \neq 0 \\ 0, & l = 0. \end{cases} \tag{A5}$$

Ideally $L = \infty$ in (A4), but in this study $L = 7$ provided an adequate amplitude response and perfect 90° phase response for frequencies between 1 cycle per 80 months and 1 cycle per 4.5 months. It was found later that similar Chebyshev filters (Hermann, 1969) would have had less "ripple" contamination than (A5) with $L = 7$. Indeed ripple effects, even with $L \gg 7$, are still a property of (A5). However, we did a number of simple complex EOF analyses on known data using $\hat{u}$ formed by the Fourier method, Chebyshev convolution, and the (A5)-type convolution with $L = 7$ and 25. The principal features of the input field were recovered in every case. In future work, however, the reader is advised that the response properties of (A5) can be improved upon if so desired.

Use of the convolution methods requires (i) losing information at each end of the time series (7 points in our case). (ii) Prior to forming the complete field descriptor U [e.g., Eq. (3)] one should also operate on u with a filter whose amplitude response is similar to that of the Hilbert transformer but whose phase shift is 0. In the current study the results were insensitive to the application (or lack of it) of such a filter to u. The main information content of the data clearly resides in frequencies associated with the large bandpass region of $h(l)$ as defined in (A5).

2. Filtering operations

One may wish to concentrate attention on variability in a specific frequency band. Wallace and Dickinson (1972) used the cross spectral matrix and its eigenmodes as filtering devices to isolate desired frequency bands. Given the matrix (ϕ_{nm}) and associated eigenvectors, they "reconstruct" a component of the data set solely from information in a given frequency band of ϕ_{nm}. The estimate of ϕ_{nm} entailed first calculation of a time-lagged covariance matrix and then its Fourier transform. There are several other frequency-space filtering methods which appear potentially more efficient.

a. Fourier method

Inspection of (A3) shows $\hat{u}(t)$ to be constructed by summation over all Fourier components. Effective ω space filtering could readily be accomplished by just limiting the range of the summation to, say, $\omega_0 \pm \delta\omega$.

Problems arise if $\delta\omega$ is small and the Fourier coefficients unstable. Prior smoothing will contaminate the desired frequency band with information form surrounding regions of ω space, a fact noted by Wallace (1972). For large $\delta\omega$ (broadband pass) there is still leakage into the selected band but it is not as critical. But the difference between this method and the inherent bandpass character of $\hat{u}$ obtain via the convolution method diminishes as $\delta\omega$ increases. Finally, *what bandwidth should one choose?* Without a spectral peak or some other spectral characteristic for guidance the selection of $\omega_0 \pm \delta\omega$ is a highly subjective operation. Since most climatic spectra are "red" they offer little help in the selection process.

b. Convolution method

Bandpass filters with amplitude responses different than (A5) can easily be constructed. When applied to estimate $\hat{u}$ (and with similar filtering of u) the resulting U can be representative of nearly any frequency band one desires. The cost of this approach is loss of data from both ends of the record. But the Fourier method has this problem also. One is again faced with the question of what bandpass to choose.

3. Generalization to vector fields

The analysis described in Section 3 may be extended to vector fields of any dimension. Consider, for simplicity, a field composed of the two-dimensional wind velocity anomaly components denoted by (u, v). Then form

$$\left.\begin{aligned} U &= u + i\hat{u} \\ V &= v + i\hat{v} \end{aligned}\right\} \tag{A6}$$

as before. Both U and V are defined at common spatial points $x_j = 1, 2, \ldots, \mathrm{NP}$ and temporal points $t_k, = 1, 2, \ldots, \mathrm{NT}$. Next form a composite series W from (A6) such that

$$\left.\begin{aligned} W(x_j, t_k) &= U(x_j, t_k), \quad j = 1, 2, \ldots, \mathrm{NP} \\ W(x_{j+\mathrm{NP}}, t_k) &= V(x_j, t_k), \quad k = 1, 2, \ldots, \mathrm{NT} \end{aligned}\right\}. \tag{A7}$$

The resulting new variable $W(x_l, t_m)$ is now defined on the interval $l = 1, 2, \ldots, 2\mathrm{NP}$ and $m = 1, 2, \ldots, \mathrm{NT}$.

The covariance matrix C [Eq. (5)] is defined as before except it will now have dimension $2\mathrm{NP} \times 2\mathrm{NP}$ and include cross products of U and V. The analysis proceeds as above but the interpretation of the results is modified in the following ways:

- The analysis is extracting the simultaneously covarying patterns of the vector components (u, v).
- The eigenvectors (B_n) are orthonormal only when dotted over their full 2NP components.

• The first NP elements of the B_n refer to the spatial covariability of the u components in the vector field, while the last NP elements refer to the *simultaneous* covariations of the v-components; similarly with the spatial phase and variance measures [Eqs. (9) and (10), respectively].

• The vector field variance associated with each mode (n) is still given by $\lambda_n/\Sigma\ \lambda_m$. However, this variability is partitioned between the (u, v) components in the ratio

$$R_{uv} = \frac{\sum_{j=1}^{NP} B_n(x_j)B_n^*(x_j)}{\sum_{j=NP+1}^{2NP} B_n(x_j)B_n^*(x_j)}. \quad \text{(A8)}$$

• The simultaneous spatial covariability of the vector components (u, v), as expressed in the $B_n(x_j)$, $j = 1, 2, \ldots, 2NP$, is modulated by a single principal component $A_n(t)$. This variable is obtained through (8) where now the summation extends over all 2NP spatial points. The orthogonal properties and scaling of the $A_n(t)$ are unchanged.

• One measure of spatial phase for variations in the vector field, say, $\theta'_n(\mathbf{x})$, is obtained from the equivalent of (9) by using a "composite" eigenvector B'_n in place of B_n, where $B'_n(x_j) = B_n(x_j) + B_n(x_{j+NP})$, $j = 1, 2, \ldots, NP$ and hence

$$\theta'_n(\mathbf{x}) = \arctan\left[\frac{\mathrm{Im}B'_n}{\mathrm{Re}B'_n}\right]. \quad \text{(A9)}$$

REFERENCES

Anderson, J. R., 1982: Space-time structure of changes in atmospheric angular momentum M.S. thesis, Dept. Meteor. Phys. Oceanogr., MIT, 77 pp.

Barnett, T. P., 1977: The principal time and space scales of the Pacific Trade Wind field. *J. Atmos. Sci.*, **34**, 221–235.

——, 1981: Statistical relations between ocean and atmosphere fluctuations in the tropical Pacific. *J. Phys. Oceanogr.*, **11**, 1043–1058.

Bergland, G. D., 1969: A guided tour of the fast Fourier transform. Reprinted in *Digital Signal Processing*, L. R. Robins and C. M. Roder, Eds. IEEE Press, 1972.

Berlage, H. P., 1966: The Southern Oscillation and world weather. Koninklijk Nederlands Meteorologisch Instituut, De Bilt, *Mededelingen en Verhandelingen*, No. 88, 152 pp.

Bjerknes, J., 1966: A possible response of the atmospheric Hadley circulation to equatorial anomalies of ocean temperature. *Tellus*, **18**, 820–829.

Busalacchi, A. J., and J. J. O'Brien, 1981: Interannual variability of the equatorial Pacific in the 1960's. *J. Geophys. Res.*, **86**, 10 901–10 907.

Cane, M. A., and E. S. Sarachik, 1981: The response of a linear baroclinic equatorial ocean to periodic forcing. *J. Mar. Res.*, **39**, 651–693.

Ding, Y., and E. R. Reiter, 1981: A climatological study of some dynamical conditions influencing the variability in typhoon formation over the west Pacific Ocean. Environmental Research Papers, No. 28, Dept. Atmos. Sci., Colorado State University, Fort Collins, 15 pp.

Egger, J., G. Meyers and P. B. Wright, 1981: Pressure, wind and cloudiness in the tropical Pacific related to the Southern Oscillation. *Mon. Wea. Rev.*, **109**, 1139–1149.

Enfield, D. B., 1981: Annual and non-seasonal variability of the monthly low level wind fields over the southeastern tropical Pacific. *Mon. Wea. Rev.*, **109**, 2177–2190.

Goldenberg, S. B., and J. J. O'Brien, 1981: Time and space variability of tropical Pacific wind stress. *Mon. Wea. Rev.*, **109**, 1190–1207.

Hasselmann, K., and T. P. Barnett, 1981: Techniques of linear prediction for systems with periodic statistics. *J. Atmos. Sci.*, **38**, 2275–2283.

Hermann, Otto, 1969: Transversal filter for Hilbert-transformation. *Arch. Elektr. Ubertragung*, **23**, 581–587.

Hickey, B., 1975: Relationship between fluctuations and sea level, wind stress and sea-surface temperature in the equatorial Pacific. *J. Phys. Oceanogr.*, **5**, 460–475.

Jenkins, G. M., and D. G. Watts, 1968: *Spectral Analysis and Its Applications*. Holden-Day, 525 pp.

McCreary, J., 1976: Eastern tropical ocean response to changing wind systems with application to El Niño. *J. Phys. Oceanogr.*, **6**, 632–645.

Meyers, G., 1982: Interannual variations in sea level near Truk Island—A bimodal seasonal cycle. *J. Phys. Oceanogr.*, **12**, 1161–1168.

Oppenheimer, A. V., and R. W. Schafer, 1975: *Digital Signal Processing*. Prentice Hall, 360 pp.

Pazen, S. E., and G. Meyers, 1982: Interannual fluctuations of the tropical Pacific wind field and the Southern Oscillation. *Mon. Wea. Rev.*, **110**, 587–600.

Philander, S. G. H., 1979: Variability of the tropical oceans. *Dyn. Atmos. Oceans*, **3**, 191–208.

Preisendorfer, R. W., F. W. Zwiers and T. P. Barnett, 1981: Foundations of principal component selection rules. SIO Ref. Ser. 81-4, Scripps Institution of Oceanography, La Jolla, CA, 192 pp.

Rasmusson, E. M., P. A. Arkin, W. Y. Chen and J. B. Jalickee, 1981: Biennial variations in surface temperature over the United States as revealed by singular decomposition. *Mon. Wea. Rev.*, **109**, 181–192.

——, and T. H. Carpenter, 1982: Variations in tropical sea surface temperature and surface wind fields associated with the Southern Oscillation/El Niño. *Mon. Wea. Rev.*, **110**, 354–384.

Sadler, J. C., and B. E. Harris, 1970: The mean tropospheric circulation and cloudiness over southeast Asia and neighboring areas. Sci. Rep. No. 1, Air Force Cambridge Research Laboratories, 38 pp.

Thomas, J. B., 1969: *An Introduction to Statistical Communication Theory*, Wiley, 663 pp.

Trenberth, K. E., 1976: Spatial and temporal variations of the Southern Oscillation. *Quart. J. Roy. Meteor. Soc.*, **102**, 639–653.

Wallace, J. M., 1972: Empirical orthogonal representation of time series in the frequency domain, Part II, Application to the study of tropical wave disturbances. *J. Appl. Meteor.*, **11**, 893–900.

——, and R. E. Dickinson, 1972: Empirical orthogonal representation of time series in the frequency domain, Part I, Theoretical considerations. *J. Appl. Meteor.*, **11**, 887–892.

Weare, B. C., 1981: Moisture variations associated with El Niño events. *Proc. Symp. Variations in the Global Water Budget*, D. Rydel (in press).

Wyrtki, K., 1975: El Niño—The dynamic response of the equatorial Pacific to atmospheric forcing. *J. Phys. Oceanogr.*, **5**, 572–584.

——, and G. Meyers, 1975a: The Trade Wind field over the Pacific Ocean, Part I: The mean field and the mean annual variation. HIG-75-1, Hawaii Institute of Geophysics, 51 pp.

——, and ——, 1975b: The Trade Wind field over the Pacific Ocean, Part II: Bimonthly fields of wind stress: 1950 to 1972. HIG-75-2. Hawaii Institute of Geophysics, 155 pp.